

1 Sources of Pressure in Titan's Plasma Environment

N. Achilleos,^{1,3,6} C. S. Arridge,^{2,3} C. Bertucci,⁵ P. Guio,^{1,3} N. Romanelli,⁵ N.

Sergis⁴

arXiv:1312.3845v1 [astro-ph.EP] 13 Dec 2013

N. Achilleos, Department of Physics and Astronomy, University College London, Gower Street,
London WC1E 6BT, UK. (nicholas.achilleos@ucl.ac.uk)

¹Department of Physics and Astronomy,

2 In order to analyze varying plasma conditions upstream of Titan, we have
3 combined a physical model of Saturn's plasmadisk with a geometrical model
4 of the oscillating current sheet. During modeled oscillation phases where Ti-
5 tan is furthest from the current sheet, the main sources of plasma pressure

University College London, Gower Street,

London, UK

²Mullard Space Science Laboratory,

Holmbury St. Mary, Dorking, Surrey, UK

³Centre for Planetary Sciences at UCL /

Birkbeck, University College London,

Gower Street, London, UK

⁴Office for Space Research and

Technology, Academy of Athens, Athens,

Greece

⁵Instituto de Astronomía y Física del

Espacio, University of Buenos Aires, Buenos

Aires, Argentina

⁶Visiting professor at Japan Aerospace

Exploration Agency Institute of Space and

Astronautical Science (ISAS), Sagamihara,

JAPAN

6 in the near-Titan space are the magnetic pressure and, for disturbed con-
7 ditions, the hot plasma pressure. When Titan is at the center of the sheet,
8 the main source is the dynamic pressure associated with Saturn's cold, sub-
9 corotating plasma. Total pressure at Titan (dynamic plus thermal plus mag-
10 netic) typically increases by a factor of five as the current sheet center is ap-
11 proached. The predicted incident plasma flow direction deviates from the or-
12 bital plane of Titan by $\lesssim 10^\circ$. These results suggest a correlation between
13 the location of magnetic pressure maxima and the oscillation phase of the
14 plasmashield.

1. Introduction

15 Titan is usually embedded within the rotating magnetosphere of Saturn - a configuration
16 which leads to the formation of a ‘flow-induced’ magnetosphere, via the draping of the
17 magnetic field in the subcorotating flow about the moon (Titan’s orbital speed of \sim
18 6 km s^{-1} is small compared to the typical speed of the rotating plasma, $\sim 120 \text{ km s}^{-1}$).
19 Recently, *Bertucci et al.* [2009] demonstrated, using *Cassini* data, that the direction and
20 magnitude of the magnetic field upstream of Titan varies, depending mainly on whether
21 Titan is located above or below Saturn’s magnetospheric current sheet. Titan’s distance
22 from the current sheet is influenced by global magnetospheric oscillations at Saturn, which
23 change the elevation of this structure with respect to the rotational equatorial plane. The
24 sheet geometry was modeled by *Arridge et al.* [2011b] (hereafter A11).

25 In Figure 1, we plot one example of current sheet elevation, Z_{CS} , from this A11 model.
26 For constant radial distance (e.g. along Titan’s orbit), Z_{CS} will vary with azimuth - i.e.
27 there is a ‘ripple’ in the sheet surface. For southern summer, Z_{CS} is everywhere positive
28 - hence, the azimuthally averaged surface forms a ‘bowl-like’ shape. We have combined
29 the A11 model of sheet geometry with the Saturn plasmadisk model of *Achilleos et al.*
30 [2010a] (hereafter Ach10) in order to predict the variable magnetic and plasma parameters
31 during the T15 encounter of Titan by the *Cassini* spacecraft (closest approach occurred
32 on July 2, 2006 at 09:21 UTC, at altitude $\sim 1900 \text{ km}$). This analysis enables us to
33 predict the variations which arise from plasma sheet oscillations. In future, we aim to
34 repeat the analysis for additional Titan encounters, and so provide a theoretical analog
35 of observational classifications of the Titan environment, such as those of *Rymer et al.*

36 [2009] and *Simon et al.* [2010]. We have also chosen T15 for the present analysis because
 37 we have obtained relevant plasma moment data which we compare with our model results
 38 herein.

39 In §2, we describe a combined model which employs the A11 current sheet geometry
 40 with the Ach10 magnetic field / plasma model. In section §3, we implement this model
 41 and compare it to observations of the magnetic field, magnetic pressure and hot plasma
 42 pressure for several magnetospheric oscillation periods centered on the T15 Titan flyby
 43 (hot plasma pressure refers to H+ and O+ ions with energies > 3 keV [*Sergis et al.*, 2009]).
 44 We summarize and give conclusions in §4.

2. Plasmadisk Model Description

45 For this study, we require a ‘two-component’ model of Saturn’s plasmadisk. The first
 46 component is the A11 geometrical model of the current sheet, illustrated in Figure 1. For
 47 cylindrical radial distance exceeding $\sim 12 R_S$, the altitude Z_{CS} of the current sheet (with
 48 respect to Saturn’s rotational equator) is given by A11:

$$Z_{CS} = [(\rho - R_H \tanh(\rho/R_H))] \tan(-\theta_{\odot}) + \tan(\theta_T) (\rho - \rho_o) \cos(\lambda), \quad \rho > 12R_S \quad (1)$$

49 where the first term represents the axisymmetric bowl and the second term the spatial
 50 oscillation, or ripple. Symbols have the following meanings: ρ is cylindrical radial distance
 51 with respect to the planet’s rotational / magnetic axis, R_H is the hinging distance which
 52 controls the curvature of the bowl, θ_{\odot} is the subsolar latitude at Saturn, θ_T is an effective
 53 angle of tilt for the current sheet, $\rho_o = 12R_S$ is a scaling distance which controls the

54 amplitude of the ripple. λ represents the following phase angle for describing plasma
 55 sheet oscillation, dependent on both position and time:

$$\lambda = \lambda_{SLS3} - \lambda_o - \Omega_{SKR}(\rho - \rho_o)/V_{WAVE}, \quad (2)$$

56 where SLS3 denotes the longitude of *Kurth et al.* [2008], based on fitting a low-order
 57 polynomial to the non-stationary period of the Saturn Kilometric Radiation (SKR). Since
 58 SLS3 was developed, distinct SKR signals have been identified in Saturn’s northern and
 59 southern hemisphere (e.g. *Lamy* [2011]) - the SLS3 phase lies consistently within $\sim 30^\circ$
 60 of that of the southern SKR source [*Andrews et al.*, 2010]. λ_o denotes a ‘prime meridian’
 61 parameter, fitted by A11 to different passes of *Cassini* data. Ω_{SKR} is a variable angular
 62 velocity corresponding to the SLS3 period. V_{WAVE} is a ‘wave speed’ parameter which
 63 introduces a systematic delay of the oscillation phase with radial distance (see Figure 1).
 64 The T15 Titan encounter occurred during *Cassini*’s Revolution 25. We thus adopt the
 65 same sheet parameters as used by A11 for their Rev 25 model fit, namely $\lambda_o = 100^\circ$,
 66 $V_{WAVE} = 5 R_S \text{ hr}^{-1}$, $R_H = 16 R_S$, $\theta_T = 12^\circ$, $\rho_o = 12 R_S$.

67 The second component of our plasmadisk model specifies magnetic field and plasma
 68 distributions for an axisymmetric magnetosphere in which magnetic force, centrifugal
 69 force and plasma pressure forces are in equilibrium (Ach10). This model also assumes
 70 north-south symmetry, with a current sheet lying in the rotational equator. Any plasma
 71 parameter is a function of two coordinates, labeled ρ_μ and Z_μ , the respective cylindrical
 72 radial distance and altitude (with respect to the rotational equator) in the ‘Ach10 model

73 space’. In order to combine the Ach10 model with the A11 sheet geometry, we calculate
 74 ‘equivalent Ach10 model coordinates’ corresponding to the spacecraft’s actual location:

$$\begin{aligned} \rho_\mu &= \rho_{S/C} \\ Z_\mu &= (Z_{S/C} - Z_{CS}) \hat{\mathbf{z}} \cdot \hat{\mathbf{n}}, \end{aligned} \quad (3)$$

75 where $\rho_{S/C}$ is the spacecraft’s actual cylindrical radial distance from the planet’s rotation
 76 / dipole axis, $Z_{S/C}$ and Z_{CS} are the respective altitudes of the spacecraft and the A11
 77 current sheet with respect to the rotational equator, $\hat{\mathbf{z}}$ is a unit vector pointing in the
 78 northern direction of the planet’s axis, and $\hat{\mathbf{n}}$ is the unit vector normal to the A11 current
 79 sheet at the distance $\rho = \rho_{S/C}$. These expressions assume that the local structure of the
 80 plasmadisk (at *Cassini*) may be approximated by a version of the Ach10 model, whose
 81 plane of symmetry has been rotated to match the local tangent plane of the A11 sheet.

3. Comparison of Plasmadisk Models and T15 Observations

82 In Figure 2, we show the observed and modeled components of the magnetic field in
 83 cylindrical coordinates. The two Ach10 model parameters explored, in order to fit the
 84 data, are the effective magnetodisk radius R_{DISK} and a proxy for the ring current activity
 85 which makes use of the global hot plasma pressure, based on multi-orbit statistics of the
 86 pressure moments from the *Cassini* Magnetospheric Imaging Instrument (MIMI) instru-
 87 ment (see *Achilleos et al.* [2010b]; *Sergis et al.* [2007]). The fit shown is for $R_{\text{DISK}} = 40 R_S$
 88 and average ring current (equivalent to hot plasma pressure $P_H = 2 \times 10^{-3}$ nPa at Titan’s
 89 orbit). The r.m.s. difference between the data and model (summed over radial and az-
 90 imuthal components, for the time interval plotted) changes by $\sim 30\%$ for corresponding

91 changes $\Delta R_{\text{DISK}} = 5 R_S$ and $\Delta P_H = 2.5 \times 10^{-4}$ nPa. We show several magnetospheric
 92 oscillations. The fits to the amplitude and phase of the B_ρ (radial) and B_ϕ (azimuthal)
 93 fields are reasonable, although: (i) Earlier B_ρ data show a change in sign, indicative of
 94 passage north of the current sheet plane, which is not reproduced with the model; (ii)
 95 The B_ϕ fluctuations show a much steeper ‘rising’ part compared to the model, suggest-
 96 ing that the plasmashet ripple exhibits structure more complex than a sinusoidal form
 97 (equation 1). The model B_Z is almost in antiphase with the observation, also suggesting
 98 additional plasmashet structure beyond our ‘wavy disk’ model (e.g. a rotating azimuthal
 99 anomaly in hot pressure has been proposed by *Brandt et al.* [2010]).

100 In Figure 3a, we show model plasma parameters corresponding to the field model of
 101 Figure 2. The vertical velocity V_Z of the plasmashet is similar for Titan and *Cassini*
 102 reference frames near closest approach, with values up to ~ 30 km s⁻¹. Similar vertical
 103 velocities were measured by the *Cassini* plasma spectrometer (CAPS) during the T15
 104 flyby [*Sillanpää et al.*, 2011]. The azimuthal velocity of the cold plasma, lying on field
 105 lines conjugate with the spacecraft, is shown in the middle panel. The largest northward
 106 excursions of the plasmashet (zero-crossing points which occur after the positive maxima
 107 in V_Z) are accompanied by decreases in V_ϕ as the spacecraft moves away from the current
 108 sheet, and connects to flux tubes extending to larger radial distances, which rotate more
 109 slowly. Note that V_ϕ for the interval shown, combined with the V_Z for the Titan frame,
 110 indicate that the upstream plasma flow direction is tilted with respect to the rotational
 111 equator by angles $\lesssim 12^\circ$. The location of maximum magnetic pressure along draped

112 flux tubes would also be expected to deviate from the rotational equator, for appropriate
 113 oscillation phases.

114 The observed magnetic field is dominantly radial outside the current sheet. The max-
 115 imum value of $|B_\rho/B_Z|$ for the interval shown is ~ 20 , which also equals the maximum
 116 ratio $|E_Z/E_\rho|$ for the convective electric field (see *Arridge et al.* [2011a] for more details).

117 In the bottom panel of Figure 3a, we show the contributions to plasma pressure from
 118 various sources. The maximum pressure during current sheet encounters is provided by the
 119 dynamic pressure of the cold, subcorotating plasma (violet curve). In the exterior regions
 120 or ‘lobes’ of the sheet, magnetic pressure shows local maxima and is the dominant pressure
 121 source for this average-ring-current model. The amplitudes and phasing of the observed
 122 fluctuations in magnetic pressure (thin gray curve) are in reasonable agreement with the
 123 model - although the narrower observed minima suggest a thinner sheet. The hot plasma
 124 pressure (red curve) shows relatively weak fluctuations compared to the other curves, since
 125 we assume that the hot population has uniform pressure all the way along the field lines.
 126 The blue curve indicates thermal pressure of the cold plasma. The total effective pressure
 127 predicted by the model (i.e. dynamic plus thermal plus magnetic) typically increases by
 128 a factor of approximately five as the current sheet center is approached. This change is
 129 mainly due to the variability in dynamic pressure between the sheet center and lobes (the
 130 relative change in pressure becomes $\sim 10\%$ if dynamic pressure is excluded).

131 In Figure 3b, we compare observed and modeled hot plasma pressure. The global profile
 132 of hot plasma pressure was increased to twice the value for the ‘disturbed ring current’
 133 of A10. Comparing the red curves (middle panel), the observed hot plasma pressure

134 outside the current sheet (local maximum in magnetic pressure) is in agreement with the
 135 model. The data show additional variability in hot pressure, due to plasma injections
 136 and ion beams, which are not explicitly modeled. This disturbed-ring-current model, in
 137 comparison to the average-ring-current case (Figure 3b), shows more comparable values
 138 of magnetic and hot pressure in the lobes of the sheet.

139 The bottom panel of Figure 3b shows model plasma beta parameters, and the observed
 140 hot plasma beta from the *Cassini* data. The model hot plasma beta (β_h) varies between
 141 $\sim 1 - 100$, while the observed β_h reaches values as low as ~ 0.01 . A ‘pseudo’ plasma beta
 142 may be defined for the dynamic pressure (Ach10) according to $\beta_d = P_{\text{dyn}}/P_{\text{mag}}$, where
 143 subscripts indicate dynamic and magnetic pressures. β_d shows local maximum values
 144 comparable to those for β_h . The thermal cold plasma beta, β_c , shows the lowest values,
 145 down to $\sim 10\%$ of β_h . The ratio β_c/β_d has similar minimum values, since the bulk kinetic
 146 energy of the cold plasma ions far exceeds their thermal energy.

4. Conclusions

147 We have calculated a plasmadisk model for conditions at the orbit of Titan during the
 148 T15 encounter by *Cassini*. Our model reproduces some of the large-scale variability in
 149 the observed magnetic field, although more complex structure for the ripple in the current
 150 sheet is required for better agreement. The model outputs are in reasonable agreement
 151 with the *Cassini* observations of magnetic pressure and hot plasma pressure.

152 For magnetospheric oscillation phases where Titan is furthest from the current sheet,
 153 the field is strongly radial and the dominant source of pressure is the dynamic pressure of
 154 the subcorotating, cold plasma. For phases where Titan is near the center of the sheet,

155 the dominant pressure sources are the magnetic and hot plasma pressures (the latter
156 being prevalent for the disturbed ring current of T15). Magnetospheric oscillations also
157 control changes in vertical and azimuthal velocities of the cold plasma for a Titan-based
158 observer. In our model, the incident direction of cold plasma flow may be displaced from
159 Titan’s orbital plane by angles of the order $\sim 10^\circ$. This result is in good agreement with
160 observations of the plasma flow velocity by *Sillanpää et al.* [2011].

161 Finally, the plasmadisk oscillations lead to a wide range of plasma beta regimes in which
162 Titan may be immersed. The hot plasma beta may be as high as ~ 100 for phases when
163 Titan is at the center of the disk. The cold plasma beta is lower by factors of $\sim 5 - 10$. A
164 ‘pseudo’ plasma beta associated with the cold plasma bulk rotation (dynamic pressure)
165 exceeds even the hot plasma beta near the disk center.

166 This variability in plasma conditions presents a complex requirement for upstream
167 boundary conditions, such as those used in more sophisticated MHD models of the plasma
168 flow. Our model is also useful for predicting plasma moments, when observations of these
169 are scarce, or when only magnetic observations are available.

170 **Acknowledgments.** We acknowledge the continued collaboration of the *Cassini* mag-
171 netometer (MAG) and plasma (CAPS, MIMI) instrument teams. NA was supported by
172 both a JAXA Visiting Professorship and UK STFC Consolidated Grant ST/J001511/1
173 (UCL Astrophysics). CB acknowledges the financial support of the Europlanet Visiting
174 Researcher programme.

References

- 175 Achilleos, N., P. Guio, and C. S. Arridge, A model of force balance in Saturn's magne-
176 todisc, *MNRAS*, *401*, 2349–2371, doi:10.1111/j.1365-2966.2009.15865.x, 2010a.
- 177 Achilleos, N., P. Guio, C. S. Arridge, N. Sergis, R. J. Wilson, M. F. Thomsen, and A. J.
178 Coates, Influence of hot plasma pressure on the global structure of Saturn's magne-
179 todisk, *Geophys. Res. Lett.*, , *37*, L20201, doi:10.1029/2010GL045159, 2010b.
- 180 Andrews, D. J., A. J. Coates, S. W. H. Cowley, M. K. Dougherty, L. Lamy, G. Provan,
181 and P. Zarka, Magnetospheric period oscillations at Saturn: Comparison of equatorial
182 and high-latitude magnetic field periods with north and south Saturn kilometric ra-
183 diation periods, *Journal of Geophysical Research (Space Physics)*, *115*(A14), A12252,
184 doi:10.1029/2010JA015666, 2010.
- 185 Arridge, C. S., N. Achilleos, and P. Guio, Electric field variability and classifications
186 of Titan's magnetoplasma environment, *Annales Geophysicae*, *29*, 1253–1258, doi:
187 10.5194/angeo-29-1253-2011, 2011a.
- 188 Arridge, C. S., et al., Periodic motion of Saturn's nightside plasma sheet, *J. Geophys. Res.*,
189 *116*(A15), A11205, doi:10.1029/2011JA016827, 2011b.
- 190 Bertucci, C., B. Sinclair, N. Achilleos, P. Hunt, M. K. Dougherty, and C. S. Arridge,
191 The variability of Titan's magnetic environment, *Planet. Space Sci.*, *57*, 1813–1820,
192 doi:10.1016/j.pss.2009.02.009, 2009.
- 193 Brandt, P. C., et al., Saturn's periodic magnetic field perturbations caused by a rotating
194 partial ring current, *Geophys. Res. Lett.*, , *37*, L22103, doi:10.1029/2010GL045285,
195 2010.

- 196 Kurth, W. S., T. F. Averkamp, et al., An update to a Saturnian longitude system based
197 on kilometric radio emissions, *J. Geophys. Res.*, *113*, A05,222, 2008.
- 198 Lamy, L., Variability of southern and northern periodicities of Saturn Kilometric Radia-
199 tion, *Planetary, Solar and Heliospheric Radio Emissions (PRE VII)*, pp. 38–50, 2011.
- 200 Rymer, A. M., H. T. Smith, A. Wellbrock, A. J. Coates, and D. T. Young, Discrete
201 classification and electron energy spectra of Titan’s varied magnetospheric environment,
202 *Geophys. Res. Lett.*, , *36*, L15109, doi:10.1029/2009GL039427, 2009.
- 203 Sergis, N., S. M. Krimigis, D. G. Mitchell, D. C. Hamilton, N. Krupp, B. M. Mauk,
204 E. C. Roelof, and M. Dougherty, Ring current at Saturn: Energetic particle pressure in
205 Saturn’s equatorial magnetosphere measured with Cassini/MIMI, *Geophys. Res. Lett.*,
206 *34*, L09,102, doi:10.1029/2006GL029223, 2007.
- 207 Sergis, N., S. M. Krimigis, D. G. Mitchell, D. C. Hamilton, N. Krupp, B. H. Mauk, E. C.
208 Roelof, and M. K. Dougherty, Energetic particle pressure in Saturn’s magnetosphere
209 measured with the Magnetospheric Imaging Instrument on Cassini, *J. Geophys. Res.*,
210 *114*(A13), A02,214, doi:10.1029/2008JA013774, 2009.
- 211 Sillanpää, I., et al., Cassini Plasma Spectrometer and hybrid model study on Titan’s
212 interaction: Effect of oxygen ions, *Journal of Geophysical Research (Space Physics)*,
213 *116*, A07223, doi:10.1029/2011JA016443, 2011.
- 214 Simon, S., A. Wennmacher, F. M. Neubauer, C. L. Bertucci, H. Kriegel, J. Saur, C. T. Rus-
215 sell, and M. K. Dougherty, Titan’s highly dynamic magnetic environment: A systematic
216 survey of Cassini magnetometer observations from flybys TA-T62, *Planet. Space Sci.*,
217 *58*, 1230–1251, doi:10.1016/j.pss.2010.04.021, 2010.

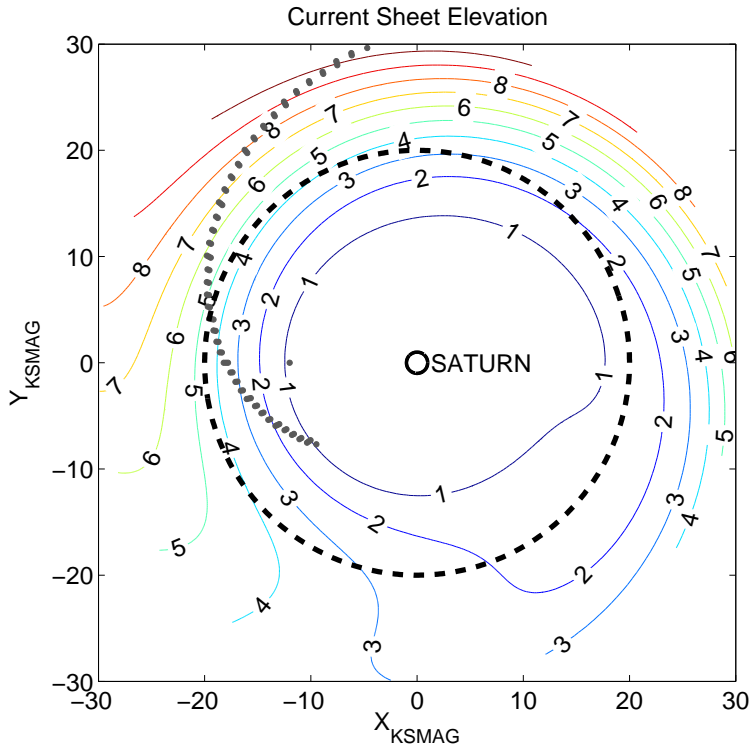


Figure 1. Plasma sheet geometry: Contours indicate the altitude Z_{CS} (in units of Saturn radii R_S) of the A11 model current sheet above Saturn’s rotational equator (see text). The geometry shown is for southern summer. The black, dashed circle is Titan’s orbit and the gray squares represent a curve of constant ‘phase’ in the sheet - this curve passes through the point of maximum Z_{CS} at each radial distance. The X_{KSMAG} axis is the intersection of the rotational equator and the noon meridian of Saturn local time (SLT). The whole pattern rotates with a variable period, following that of the SKR.

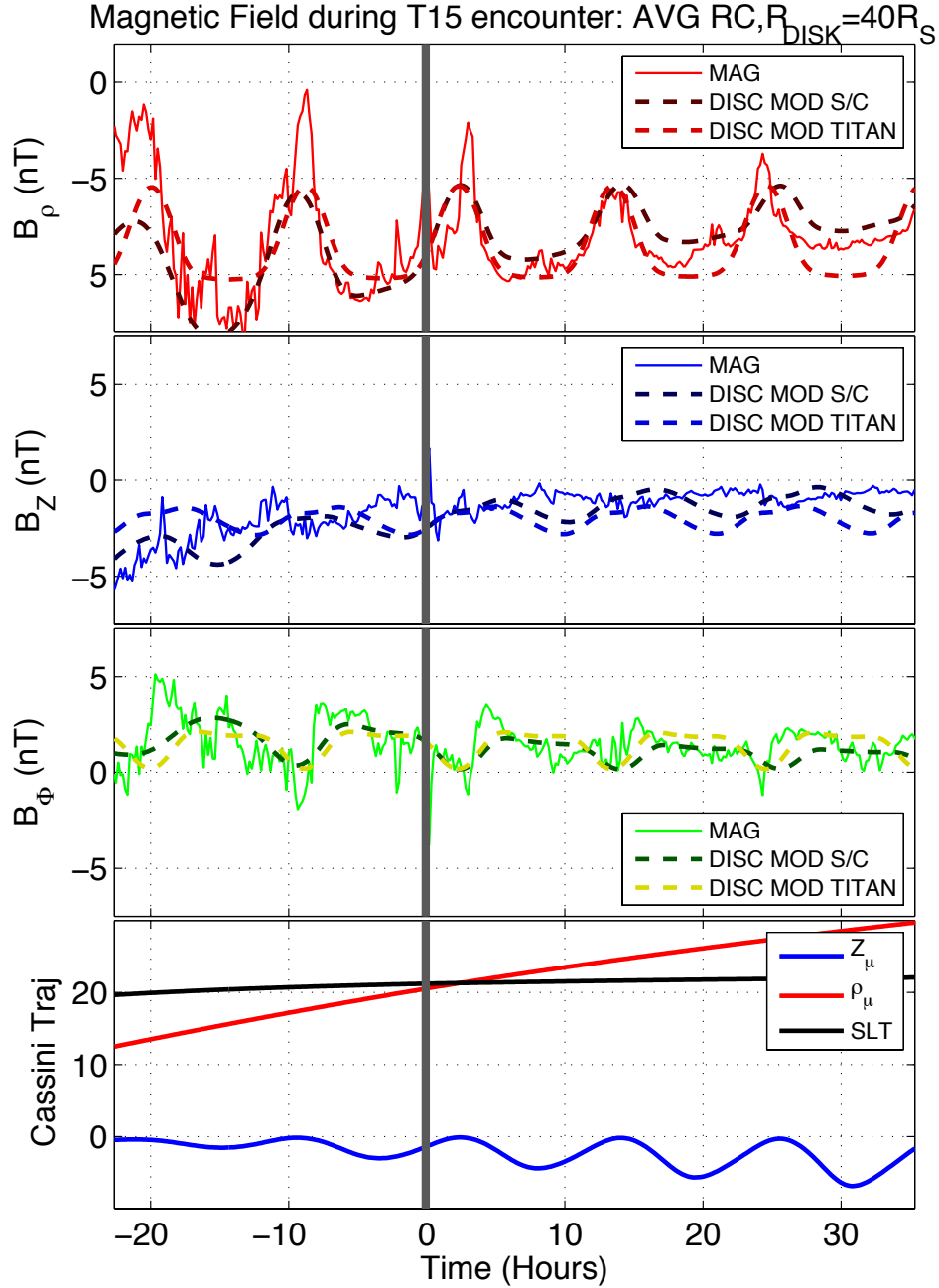


Figure 2. Top three panels: Cylindrical components of the magnetic field observed by *Cassini*, and predicted by the model, during several magnetospheric oscillations before and after the T15 wake crossing (vertical gray line). The zero of time indicates closest approach to Titan. Model fields for both *Cassini* and Titan-based observers are shown. Bottom panel: Equivalent Ach10 model coordinates along the spacecraft trajectory. Z_μ indicates perpendicular distance from the spacecraft to the A11 current sheet.

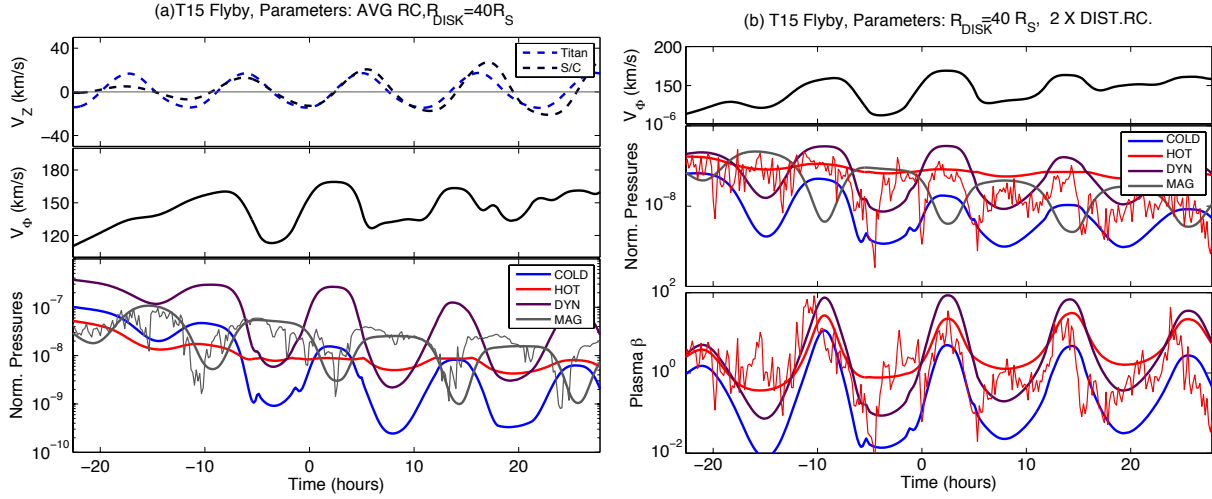


Figure 3. (a) Model predictions for a disk of effective radius $R_{\text{DISK}} = 40R_S$ and average ring current level (see text). Top panel: Predicted vertical velocity components for the plasmashet for the same time interval as Figure 2. Middle panel: Model azimuthal velocities for the cold plasma on planetary flux tubes conjugate to the spacecraft. Bottom panel: Predicted pressure contributions, color-coded according to physical origin. Pressure is normalized to the value of magnetic pressure corresponding to the equatorial surface field strength at Saturn, $B_o = 21000$ nT. (b) Model predictions for a disk of effective radius $R_{\text{DISK}} = 40R_S$ and twice the hot pressure for the ‘disturbed’ ring current level. Top panel: Azimuthal velocities for the cold plasma on planetary flux tubes conjugate to the spacecraft. Middle panel: Pressure contributions, color-coded, as for Figure 3a, according to physical origin (see text). Bottom panel: Plasma beta parameters corresponding to the model pressures and to the observed hot plasma / magnetic pressure.